SUPPLEMENTAL FIGURES AND LEGENDS

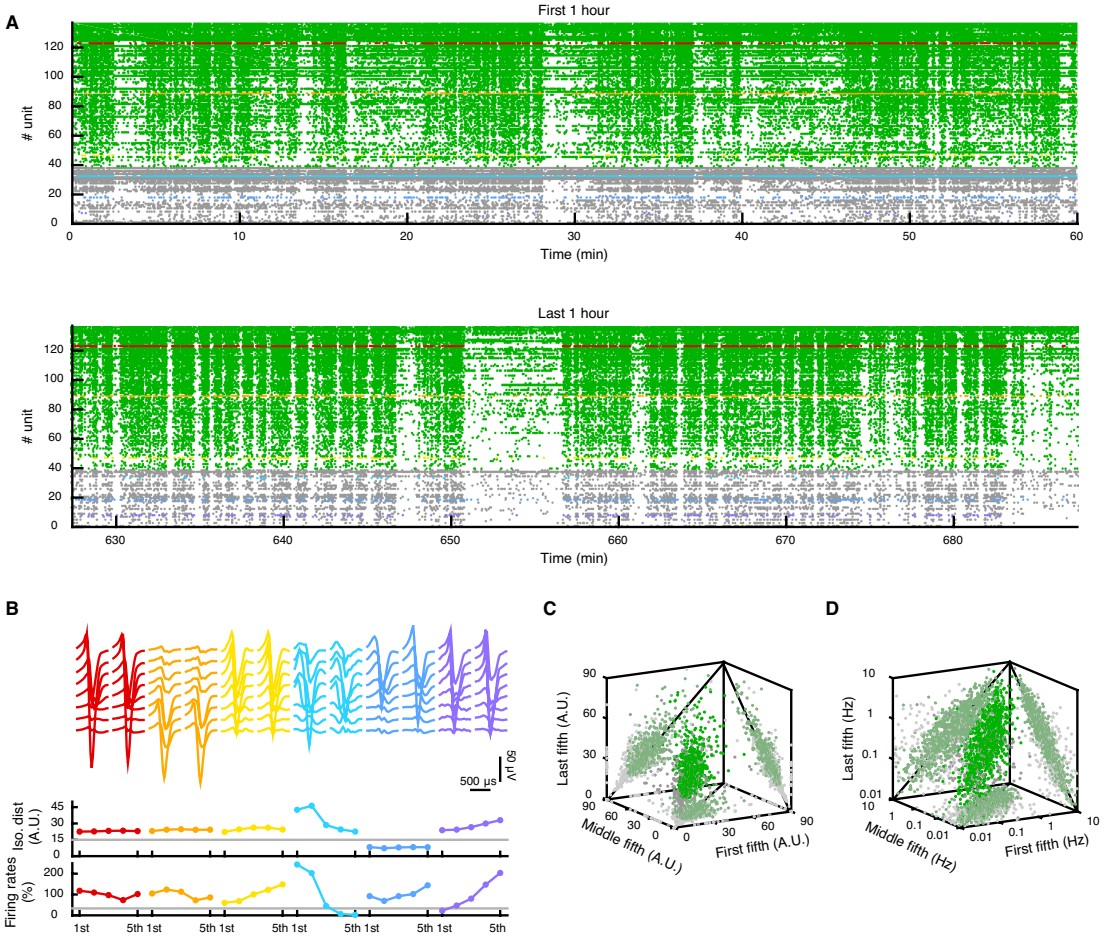

Figure S1, Stability of units in long duration recordings. Related to Experimental Procedures
(A) Raster plot of putative pyramidal cells from the first (top) and last (bottom) hours of a sample session with 98 "stable" units (green, along with specific examples in red, orange and yellow) and 39 insufficiently "stable" units (in light gray, along with specific examples in cyan, blue, and purple) in region CA1. **(B)** Sample units (colors correspond to color-matched units in panel **A**) with average waveform shown for the first (left) and last (right) fifths of the session. For this session, these fifths correspond to ~2.3 hrs, encompassing the panels shown in **A**). Isolation distance (middle) and mean firing rates (bottom) in each fifth measured as % of the session mean were used to evaluate unit stability (stable: red, orange yellow, non-stable: cyan, blue, purple). Gray lines provide criterion thresholds. **(C,D)** 3-D scatter plots of isolation distances **(C)** and mean firing rates **(D)** of stable (1017 cells, green) and insufficiently stable (352 cells, gray) putative pyramidal cells in first, middle and last fifth of session and their 2-D projections with identity (black).

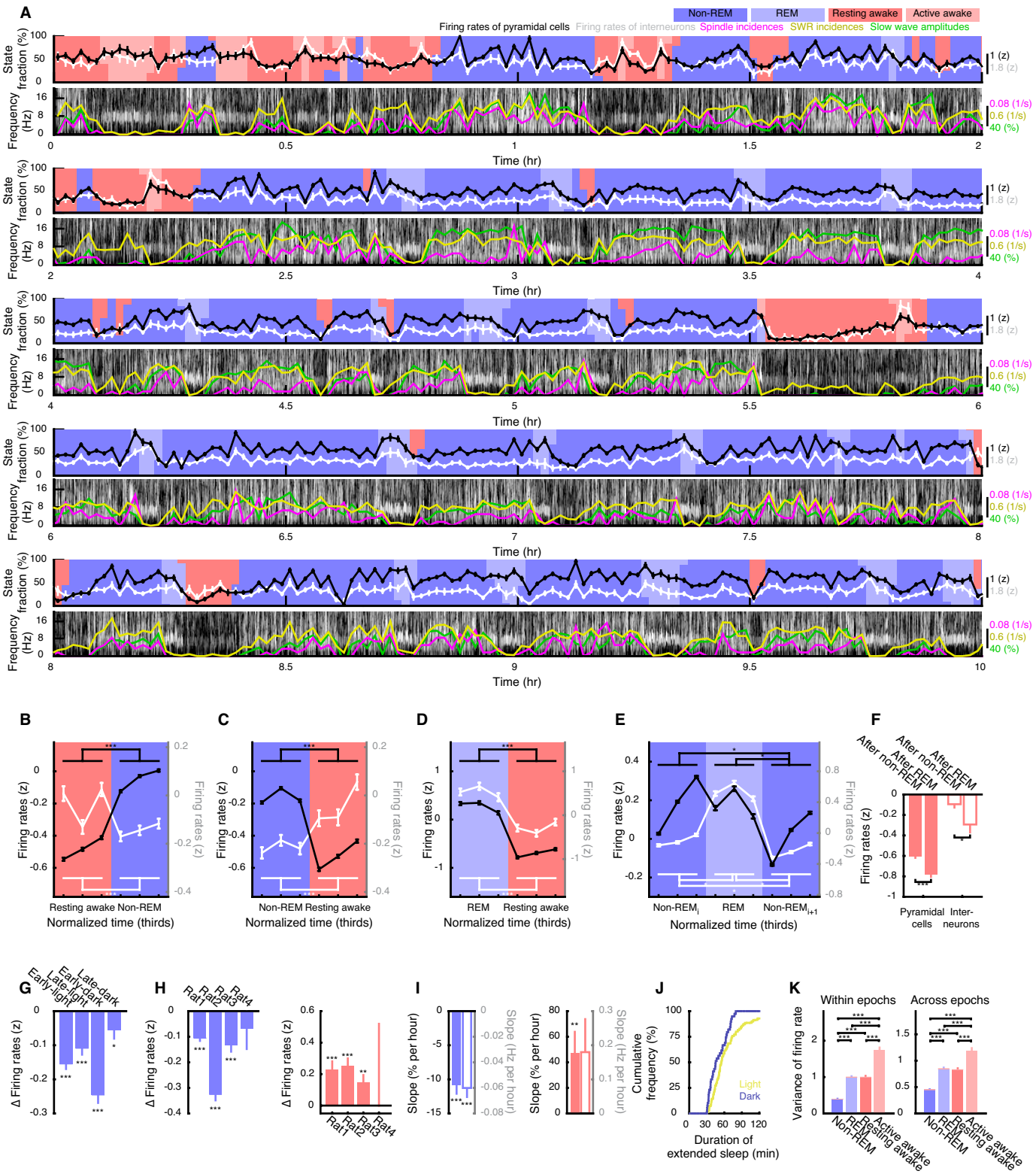

Figure S2, State-dependent firing rate changes in light and dark cycles. Related to Figure 1.

(A) Sample recording during the light cycle. Top panels of each row show the mean firing rate of 94 putative pyramidal neurons (black) and 11 putative interneurons (white), each independently z-scored for the entire session, before averaging. Background colors indicate proportion of time spent in resting awake (dark pink), active awake (light pink), non-REM (dark blue) and REM (light blue) in 1-min bins. Bottom panels of each row show the pyramidal layer LFP spectrogram (gray), with SWR incidence (yellow), spindle

incidence (magenta), and hSWA (green) averaged in each 1-min bin. **(B-E)** Mean firing rates of pyramidal cells (black, left axes) and interneurons (white, right axes) were calculated in first, middle and last one thirds of each epoch, for transitions from resting awake to non-REM (**B**, 261 transitions), non-REM to awake, (**C**, 233 transitions), REM to resting awake (**D**, 32 transitions), and non-REM_i/REM/non-REM_{i+1} triplets (**E**, 308 sequences). Mean firing rates across different epochs were compared by paired t-tests **(B-D)** or Tukey-Kramer following one-way ANOVA **(E)**. **(F)** Firing rates in both pyramidal cells and interneurons were lower in the first bin of waking following REM sleep than in waking following non-REM sleep (i.e. panel **D** vs. panel **C**; $p = 3.7 \times 10^{-10}$ for pyramidal cells and $p = 0.020$ for interneurons). **(G)** First and last non-REM epochs were separately compared in early-light (12:00 pm – 4:30 pm, 2034 cells in 37 extended sleep sequences), late-light (4:30 pm – 9:00 pm, 1292 cells in 23 sequences), early-dark (9:00 pm – 1:30 am, 1190 cells in 20 sequences) and late-dark cycles (1:30 am – 6:00 am, 1123 cells in 19 sequences) and showed significant decreases across the circadian cycle. Track running periods (9:00 am – 12:00 pm, Figure 1c) were excluded. **(H)** Consistent decreases in firing rates compared between first and last non-REM epochs over extended sleep were observed in all animals (left, {4040, 1422, 666, 77} cells in {48, 37, 17, 7} sequences for four rats). Three out of four animals also showed significantly increased firing when comparing the first and last minutes in resting awake (right, {703, 647, 819, 22} cells in {10, 18, 17, 2} stable waking episodes) **(I)** Slopes of regression for firing rates in extended sleep (left, 6205 cells in 586 non-REM epochs over 109 extended sleep episodes) were significant both when measured in percentage (filled bars, left axes) and non-normalized, in Hz (open bars, right axes). Slopes in stable waking (right, 2191 cells in 162 resting awake epochs over 47 stable waking episodes) were significant when measured in percentage. The regression slopes were calculated for each neuron per extended sleep/stable waking separately prior to averaging. **(J)** Extended sleep sequences lasted longer in light cycles (yellow) than in dark cycles (blue). **(K)** Variability of firing rates was lowest in non-REM and highest in active waking. The variance in z-scored firing rate across simultaneously recorded cells was calculated within each epoch (left panel, $n = 953$, 466, 550 and 294 epochs for non-REM, REM, resting awake and active awake, respectively). Additionally, the variance in firing rate of each cell ($n = 1017$ cells) was calculated across epochs (right panel). Statistical differences were detected by Tukey-Kramer test following one-way ANOVA ($p = 3.5 \times 10^{-196}$ for within epochs and $p = 1.9 \times 10^{-56}$ for across epochs). *$p < 0.05$, ** $p < 0.01$, *** $p < 0.001$. Error bars indicate SEM.

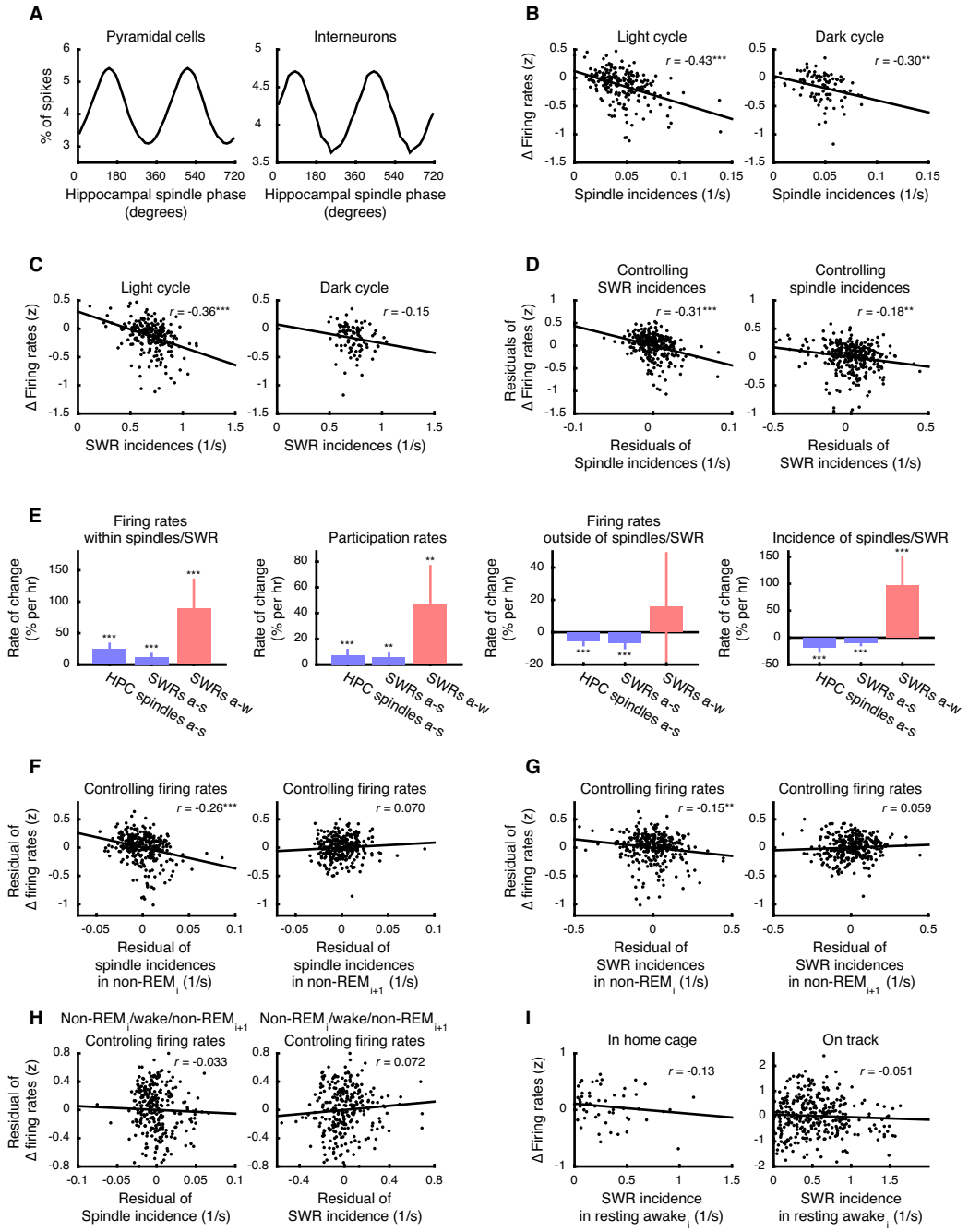

Figure S3, Spindles/SWRs modify hippocampal spiking activity. Related to Figure 2

(A) Neuronal spiking was strongly modulated by the phase of the spindle in pyramidal cells (left; 1017 cells; $p < 10^{-300}$, Rayleigh test), which fired most near the spindle trough (142.5 degrees), and in interneurons (right; 116 cells; $p < 10^{-300}$, Rayleigh test), which fired most during the descending phase of the spindle (82.5 degrees). **(B,C)** Correlation between spindle and SWR incidences in non-REM$_i$ and firing rate decreases between non-REM$_i$ and non-REM$_{i+1}$ in light (left, 217 sequences) and dark (right, 89 sequences) cycles. **(B)** Spindles were predictive of firing-rate changes in both light and dark. **(C)** SWR incidences were significantly predictive in the light cycle. **(D)** Spindles and SWRs were not redundantly predictive. Correlations were significant between firing rate decreases and SWRs [/spindles] when controlling for spindles [/SWRs]. Residuals of the linear regression for spindle incidence given SWR incidence (left panel, [spindle incidence] = 0.054 [SWR incidence] + 0.007) were significantly correlated with the residuals of the regression for firing rate changes given SWR incidence ([changes in firing rate] = –0.58 [SWR incidence] + 0.26; 306 sequences). Likewise, residuals of regression for SWR incidence given spindle incidence (right panel, [SWR incidence] = 2.9 [spindle incidence] + 0.57) were significantly correlated with the residuals of the regression for firing rate changes given spindle incidence ([change in firing rate]

= -5.34 [spindle incidence] + 0.10; 306 sequences). **(E)** Firing rates within hippocampal spindles and SWRs (left), pyramidal cell participation rates during these events (second from left), firing rates outside of these events (second from right) and the incidence rates of these events (right) were measured across sleep (a-s, 586 epochs in 109 extended sleeps) and across waking (a-w, 162 epochs in 45 stable wakings). Slopes of the corresponding regressions are shown with 95% confidence interval error bars. **(F,G)** Partial correlation analysis controlling for correlations with firing rate. **(F)** Residuals of regression for spindle incidence given firing rate during non-REM$_i$ ([spindle incidence] = 0.046 [firing rate] + 0.038) were significantly correlated with the residuals of regression for change in firing rate between non-REM$_i$ and non-REM$_{i+1}$ given firing rate during non-REM$_i$ ([change in firing rate] = –0.48 [firing rate] – 0.062; left panel, 306 sequences). In contrast, spindles in non-REM$_{i+1}$ were not predictive of firing rate changes in the time-reversed direction; no significant correlation was detected when non-REM$_i$ and non-REM$_{i+1}$ were flipped (right panel), i.e. given firing rates during non-REM$_{i+1}$ **(G)** Similarly, residuals of regression for SWR incidence given firing rate ([SWR incidence] = 0.36 [firing rate] + 0.64; 306 sequences) were correlated with residuals of regression for firing rate change given firing rate (left panel), but not in the time-reversed direction, (right panel). **(H)** In non-REM epochs separated by waking (for > 50 s), firing rate changes were not predicted by spindles/SWRS. Residuals of regression for change in firing rate given firing rate in non-REM$_i$ ([change in firing rate] = -0.63 [firing rate] + 0.050; 274 sequences) were not predicted by residuals of regression for spindle incidences given firing rate ([spindle incidence] = 0.048 [firing rate] + 0.035; left panel, 274 sequences) nor by residuals of regression for SWR incidences given firing rate (0.48 [firing rate] + 0.63; right panel, 274 sequences). **(I)** Firing rate changes between subsequent resting awake epochs interleaved by active awake were not correlated with the incidence of SWRs, neither in the home cage (left, 54 sequences) nor on the track (right, 324 sequences). ** $p < 0.01$, *** $p < 0.001$**.**

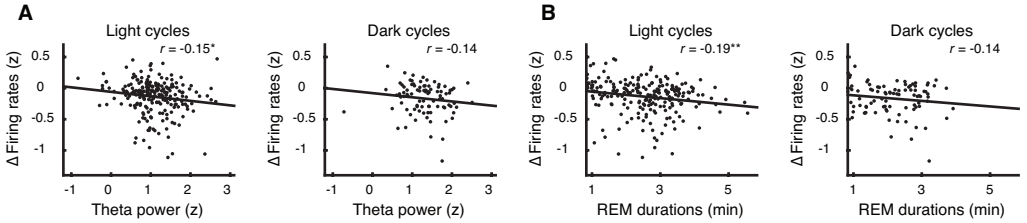

Figure S4, Changes across non-REM and interleaving REM. Related to Figure 3
Across-sleep firing rates changes between non-REM epochs were significantly correlated with mean theta power **(A)** and duration **(B)** of interleaving REM in light (left panels, 217 sequences) though not in dark cycles (right panels, 89 sequences), likely due to the smaller sample size in dark cycles. * $p < 0.05$, ** $p < 0.01$.

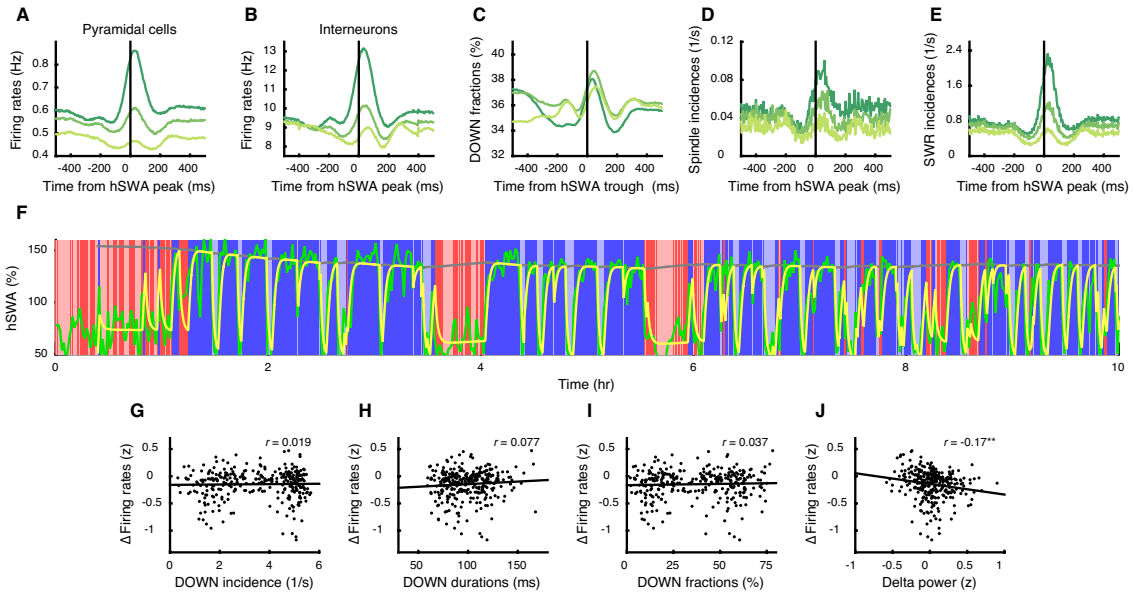

Figure S5, Slow wave patterns and firing rates. Related to Figure 4
(A,B) Mean firing rates in 5-ms bins from all sessions centered on the peak of the hippocampal slow wave (low, medium, and high amplitude thirds in corresponding shades of green) demonstrate modulation in hippocampal pyramidal cells (**A**, 1017 cells) and

interneurons (**B**, 116 cells). **(C)** Similar PETHs centered on the trough show that DOWN states are less likely immediately before, and more likely immediately after the hSWA trough. **(D,E)** PETHs triggered on the peak of the hippocampal slow wave demonstrate modulation of **(D)** hippocampal spindles and **(E)** SWRs. **(F)** The dynamics of hSWA (means in 1-min bins, green line) were well described by a process S model (yellow and gray line; see **Supplemental Experimental Procedures**). In this case, $rc = 1.2006$, $fc_R = 1.00016$, $fc_W = 0.6905$, $gc = 0.0040$, $rs = 0.0074$, $S_u = 189.1198$, $S_0 = 154.0985$, $t_a = 0.0602$, $t_p = 0.0248$, $SWA_0 = 51.3299$, and $SWA_L = 19.3145$. Background colors indicate waking/sleep states (as in **Figure 1**). **(G-I)** Changes in firing rates between non-REM$_i$ and non-REM$_{i+1}$ were not correlated with the incidence **(G)**, duration **(H)** or fraction **(I)** of hippocampal DOWN states detected in non-REM$_i$ (306 sequences). **(J)** Firing rate changes were significantly correlated with power in the delta band (< 4 Hz) during non-REM$_i$, though more weakly than with spindles/SWRs (see also multiple regression analysis in Results) ** $p < 0.01$.

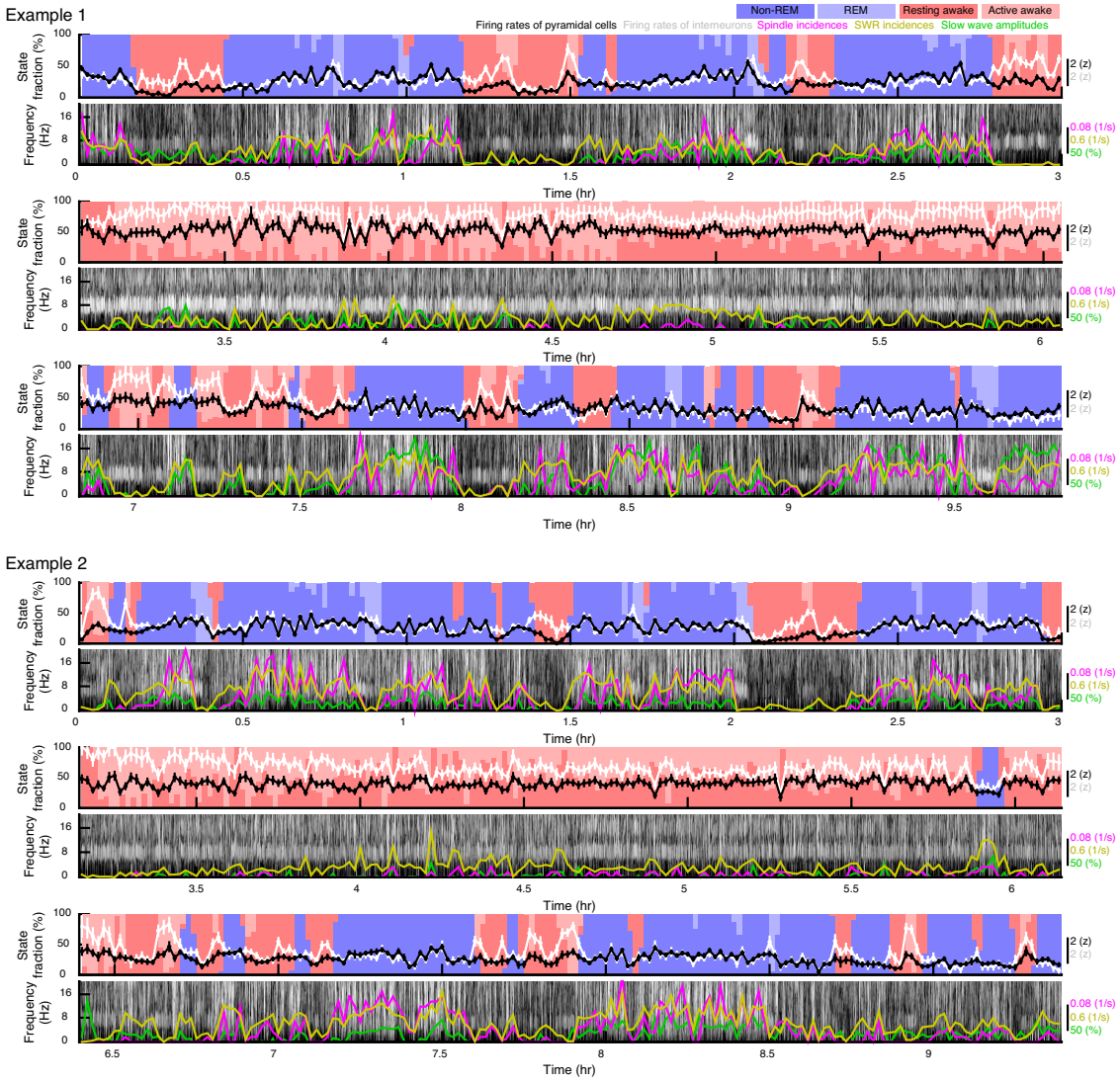

Figure S6, Hippocampal activity in two sample sessions including pre- and post-track sleep. Related to Figure 5
Top panels in each row show mean firing rates for 68 [/75] pyramidal neurons (black) and 14 [/12] interneurons (white) for top [/bottom] example, during pre-track sleep (top row), extended track running (middle row) and post-track sleep (bottom row). Background color indicates brain state (color code as in **Figure 1**). Bottom panels in each row show the hippocampal LFP spectrogram (gray), spindle incidence (magenta), and hSWAs (green).

SUPPLEMENTAL EXPERIMENTAL PROCEDURES

Animals, surgery, and data collection. All recordings were performed in freely moving and sleeping animals. Four male Long-Evans rats (250-350g; Charles River Laboratories, Wilmington, MA) were anesthetized with isoflurane and placed in a stereotaxic frame. Eight-shank "Buzsaki 64" silicon probes (NeuroNexus, Ann Arbor, MI) were implanted above the right dorsal hippocampus (2.00 mm lateral and 3.36 mm posterior from the bregma) following previously reported methods [S1]. Shanks of the silicon probe were 15 μm thick, with 8 recording sites (160 μm^2 each site, 1-3 MΩ impedance) per shank and an inter-shank distance of 200 μm. In three of the rats, 2 stainless steel wires (AS 636, Cooner wire, Chatsworth, CA) were placed into the nuchal muscles to measure the electromyograph (EMG). In two of the rats, screws were inserted on the skull above the right frontal lobe (3.00 mm lateral and 2.50 mm anterior from the bregma) and attached to Nyleze insulated copper wires (0.13 mm diameter; Alpha Wire, Elizabeth, NJ). See table summary below. The signal from the silicon probes was passed through HST/32V-G20 headstages (Plexon, Dallas, TX) connected to a Digital Lynx recording system (Neuralynx, Bozeman, MT). Silicon probes were lowered slowly over several days to the CA1 pyramidal layer. Wide-band signals were bandpass filtered (1 Hz to 9000 Hz) sampled at 30 kHz or 32 kHz and recorded continuously for >24 hrs during natural sleep and behavior. After a recovery period from surgery (> 5 days), rats were placed on a water-restriction regimen to motivate track running, and were provided with ad libitum water once daily for 30 min. All procedures were in accordance with the National Institutes of Health guidelines and approved by the University of Wisconsin-Milwaukee Institutional Animal Care and Use Committee.

Unit clustering and cell classification. Unit clustering and cell classification were performed following previously described methods [S2]. The experimental design is shown in Figure 1c. During the light cycle, animals remained in their home cage. During the dark cycle, animals were in their home cage for the first 9 hours, and then placed on the track and periodically rewarded for running over the remaining 3 hrs. Following the track session, recordings were paused for 11.8 – 45.3 (M = 23.3) minutes while recording cables were untwisted and animals were given ad libitum water. In total, we analyzed eleven 12-hr sessions and one (interrupted) 6-hr session from the light cycle, seven 9-hr sessions during the dark cycle, clustered separately. In seven additional sessions, we concatenated the data from both light and dark cycles, in order to track neurons from before, during, and after extended track running sessions. Spikes were detected following median-filtering (21-datapoint window) of the wide-band signal using NDManager and plugins [S3] (http://ndmanager.sourceforge.net), automatically sorted with KlustaKwik [S4] (http://klusta-team.github.io/klustakwik), and refined manually with Klusters [S3] (http://klusters.sourceforge.net). Putative pyramidal cells and interneurons were separated based on standard methods using waveshape, burstiness, refractory periods, and firing rates [S5, S6]. To evaluate stability of the spiking units, we measured their isolation distances [S7] and mean firing rates in 3-5 bins (bin size 2-3 hrs). Only units that met the following strict stability criteria were included in subsequent analyses: the isolation distance remained > 15 for the entire session and the firing rate within each bin did not drop more than two-thirds of the overall mean (**Figure S1**; total number of recording sessions and isolated stable cells are summarized in the table below). Firing rate z-scores were calculated using means and standard deviations (SDs) in one-min bins. We obtained similar results using non-normalized (Hz) and mean –normalized firing rate measures (e.g. see **Figure S2i**). Multiple epochs were recorded in each session, thus the same neuron contributed multiple data points in some analyses.

Spectral analyses. LFP, EMG and electroencephalogram (EEG) traces were low-pass filtered at 1250 or 1280 Hz using NDManager and plugins [S3]. Power spectra were whitened and calculated using multitaper methods with the Chronux toolbox for Matlab [S8] in 1-s windows. Additionally, the discrete wavelet transform (84 levels, 1-300 Hz) was performed using MATLAB wavelet software provided by C. Torrence and G. Compo (http://paos.colorado.edu/research/wavelets/). Power at each level of the wavelet transform was individually z-scored.

Sleep and behavioral state detection. Sleep and waking were separated based on EMG and the animal's movement. Sleep was detected by low EMG power and no movement (defined below). The remainder was considered waking. EMG signals were first smoothed with a 1-s Gaussian filter and power was z-scored in 500-ms overlapping windows at 100-ms steps. A two-threshold "Schmitt" trigger was used to detect transitions between "low" and "high" EMG power at 0 and 0.5 threshold z scores. Similarly, the thresholds for "no movement" and "movement" were set at 0.5 cm/s and 5 cm/s. Transient (< 10 s) low or high EMG power or movement states were ignored. Detected states underwent post-hoc visual inspection and occasional manual modification. In one rat for which EMG was not recorded, no movement followed by slow waves signaled non-REM sleep. REM was inferred from high theta (described below) with no movement sandwiched between non-REM epochs. Transitions from non-REM to resting awake were identified at time points when the mean hippocampal slow wave amplitude (defined below in 5-s bins) dropped < 80% of the maximum reached in the non-REM epoch. Data from this animal was consistent with the rest.

The theta (5-10 Hz) over (1-4 Hz plus 10-14 Hz) band ratio of the power spectral density was used to detect transitions between high theta and low theta, using custom-made MATLAB software written by Anton Sirota [S9] based on the Hidden Markov Model Toolbox for Matlab (Kevin Murphy), followed by visual inspection. Sleep states with high theta were classified as REM (rapid eye movement) and the remainder were classified as non-REM [S10, S11]. Similarly, waking periods with high theta were labeled "active awake" and the remainder were labeled "resting awake." Only epochs > 50 s were used in further analyses.

Extended sleep/stable waking. Extended sleep was defined as sleep which lasted > 30 mins without interruptions > 1 min. Similarly, stable waking in the home cage was defined as waking lasting >15 min without sleep interruptions > 1 min. Mean spike rates were calculated separately for each epoch of non-REM, REM, resting awake, and active awake.

Summary of data

	Rat1	Rat2	Rat3	Rat4
Recorded nuchal EMG	Yes	Yes	No	Yes
Recorded neocortical EEG	No	Yes	No	Yes
#Light/Dark sessions	4/3	4/3	3/1	1/0
#Track sessions	3	3	1	0
#Pyramidal cells/interneurons	799/123	350/15	209/22	11/0
#Non-REM/REM epochs	349/165	383/194	169/68	52/39
#Resting/active awake epochs	183/64	208/116	128/105	31/9
#Extended sleeps/stable wakings	48/10	37/18	17/17	7/2

Sharp wave ripple detection. Sharp wave ripples (SWRs) were detected following previously described methods [S12]. First, the ripple band (130-230Hz) power of the LFP was calculated during non-REM and "resting awake" states. Channels with the largest power in the ripple band were selected for each shank, and periods with power > 1 SD of the mean in one or more of these channels were labeled candidate events. Candidates with short gaps (< 50ms) were combined. Candidates < 30 ms or > 450 ms were abandoned. Remaining candidates were classified as SWRs if their peak power was > 5 SDs from the mean. For each SWR event, participation ratios were determined using the fraction of cells that emitted at least one spike.

Sleep spindle detection. Hippocampal LFP and neocortical EEG were band-pass filtered (9 - 18 Hz). For hippocampal spindles, the channel with the largest mean power in this band during non-REM was used. Candidate spindles were detected when amplitudes of the Hilbert transform exceeded 1.5 SDs above the mean for > 350 ms [S13]. Candidates with inter-event intervals < 125 ms were concatenated. Remaining candidates with peak amplitudes < 4 SDs above the mean were abandoned. For each candidate, spindle troughs were detected. Candidates with inter-trough intervals > 125 ms (i.e. slower than 8 Hz) were discarded [S13]. To determine spindle modulation of other neuronal events (e.g. SWRs and spikes), PETHs were calculated in 20-ms bins. Spindle phases were obtained from Hilbert transforms of the filtered signal. Zero and 180 degrees mark the oscillation peak and trough, respectively.

Slow wave detection. We used methods developed and described in previous reports [S14, S15] to detect the amplitudes of slow wave activity in the neocortical EEG (nSWA) and the hippocampal LFP (hSWA). The polarity of the hippocampal LFP was inverted due to the polarity reversal relative to the EEG [S16]. Individual slow waves were detected as positive deflections between two negative deflections in the band-pass filtered signal (0.5 - 4 Hz). Slow waves separated by < 100-ms were discarded. Slow wave amplitudes were measured from trough to peak, normalized by the session means, and binned into 20-ms for peri-event analyses, and 5-s bins for time-course analyses. Slow wave slopes, associated with synaptic connectivity [S17], were highly correlated with slow wave amplitudes ($r = 0.92$, $p < 10^{-300}$ in the hippocampus and $r = 0.97$, $p < 10^{-300}$ in the neocortex).

UP and DOWN state detection. DOWN states during non-REM were defined as periods with no CA1 units spiking for 50 ms or longer [S11, S14]. UP states were defined as intervals between DOWN states with 10 or more spikes from any combinations of CA1 neurons. We note that based on these conservative definitions UP and DOWN states were mutually exclusive but not exhaustive.

Process S model. The changing hSWA across waking and sleep was well described by the process S model [S18]. Process S is described by two differential equations:

$$\frac{dSWA}{dt} = rc\ SWA\left(1 - \frac{SWA}{S}\right)\frac{S}{S_u} - fc_R\ (SWA - SWA_L)\ R(t) - fc_W(SWA - SWA_L)\ W(t)$$

$$\frac{dS}{dt} = -gc\ SWA + rs\ (S_u - S)$$

In these equations, *SWA* is the amplitude of the slow oscillation, *rc* is rise constant of *SWA* and *S*, S_u is upper asymptote of *S*, fc_R and fc_W are fall constants of *SWA* triggered by REM and wake epochs respectively. SWA_L is the lower asymptote of *SWA* and *gc* is the gain constant of *SWA* that determines the decay of S. The first equation contains two functions, *R(t)* and *W(t),* which are set to 1 or 0 based on behavioral/sleep states at the time of *t*. *R(t)* is 1 from t_a min before onset of each REM epoch to t_p min after offset of each REM epoch and 0 at all other times. *W(t)* is 1 when an animal is awake and otherwise 0. Variables were initialized and solved as described [S18].

SUPPLEMENTAL REFERENCES

S1. Vandecasteele, M., M, S., Royer, S., Belluscio, M., Berenyi, A., Diba, K., Fujisawa, S., Grosmark, A., Mao, D., Mizuseki, K., et al. (2012). Large-scale recording of neurons by movable silicon probes in behaving rodents. J Vis Exp, e3568.

S2. Diba, K., and Buzsaki, G. (2008). Hippocampal network dynamics constrain the time lag between pyramidal cells across modified environments. J Neurosci *28*, 13448-13456.

S3. Hazan, L., Zugaro, M., and Buzsaki, G. (2006). Klusters, NeuroScope, NDManager: a free software suite for neurophysiological data processing and visualization. J Neurosci Methods *155*, 207-216.

S4. Harris, K.D., Henze, D.A., Csicsvari, J., Hirase, H., and Buzsaki, G. (2000). Accuracy of tetrode spike separation as determined by simultaneous intracellular and extracellular measurements. J Neurophysiol *84*, 401-414.
S5. Csicsvari, J., Hirase, H., Czurko, A., and Buzsaki, G. (1998). Reliability and state dependence of pyramidal cell-interneuron synapses in the hippocampus: an ensemble approach in the behaving rat. Neuron *21*, 179-189.
S6. Bartho, P., Hirase, H., Monconduit, L., Zugaro, M., Harris, K.D., and Buzsaki, G. (2004). Characterization of neocortical principal cells and interneurons by network interactions and extracellular features. J Neurophysiol *92*, 600-608.
S7. Schmitzer-Torbert, N., Jackson, J., Henze, D., Harris, K., and Redish, A.D. (2005). Quantitative measures of cluster quality for use in extracellular recordings. Neuroscience *131*, 1-11.
S8. Bokil, H., Andrews, P., Kulkarni, J.E., Mehta, S., and Mitra, P.P. (2010). Chronux: a platform for analyzing neural signals. J Neurosci Methods *192*, 146-151.
S9. Sirota, A., Montgomery, S., Fujisawa, S., Isomura, Y., Zugaro, M., and Buzsaki, G. (2008). Entrainment of neocortical neurons and gamma oscillations by the hippocampal theta rhythm. Neuron *60*, 683-697.
S10. Robinson, T.E., Kramis, R.C., and Vanderwolf, C.H. (1977). Two types of cerebral activation during active sleep: relations to behavior. Brain Res *124*, 544-549.
S11. Grosmark, A.D., Mizuseki, K., Pastalkova, E., Diba, K., and Buzsaki, G. (2012). REM sleep reorganizes hippocampal excitability. Neuron *75*, 1001-1007.
S12. Diba, K., Amarasingham, A., Mizuseki, K., and Buzsáki, G. (2014). Millisecond timescale synchrony among hippocampal neurons. J Neurosci *34*, 14984 –14994.
S13. Sullivan, D., Mizuseki, K., Sorgi, A., and Buzsaki, G. (2014). Comparison of sleep spindles and theta oscillations in the hippocampus. J Neurosci *34*, 662-674.
S14. Vyazovskiy, V.V., Olcese, U., Lazimy, Y.M., Faraguna, U., Esser, S.K., Williams, J.C., Cirelli, C., and Tononi, G. (2009). Cortical firing and sleep homeostasis. Neuron *63*, 865-878.
S15. Vyazovskiy, V.V., Cirelli, C., and Tononi, G. (2011). Electrophysiological correlates of sleep homeostasis in freely behaving rats. Prog Brain Res *193*, 17-38.
S16. Nir, Y., Staba, R.J., Andrillon, T., Vyazovskiy, V.V., Cirelli, C., Fried, I., and Tononi, G. (2011). Regional slow waves and spindles in human sleep. Neuron *70*, 153-169.
S17. Esser, S.K., Hill, S.L., and Tononi, G. (2007). Sleep homeostasis and cortical synchronization: I. Modeling the effects of synaptic strength on sleep slow waves. Sleep *30*, 1617-1630.
S18. Achermann, P., Dijk, D.J., Brunner, D.P., and Borbely, A.A. (1993). A model of human sleep homeostasis based on EEG slow-wave activity: quantitative comparison of data and simulations. Brain Res Bull *31*, 97-113.